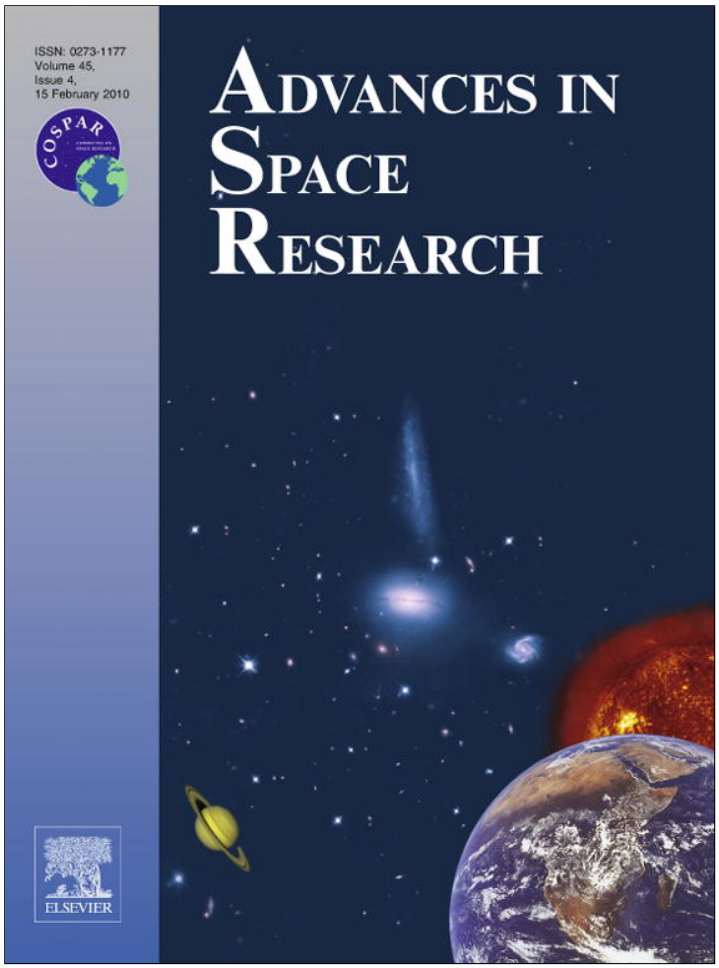

Available online at www.sciencedirect.com
ScienceDirect
Advances in Space Research 45 (2010) 527–536
ADVANCES IN SPACE RESEARCH (a COSPAR publication)
www.elsevier.com/locate/asr

Large-scale waves in the solar corona: The continuing debate

Alexander Warmuth *

Astrophysikalisches Institut Potsdam, An der Sternwarte 16, D 14482 Potsdam, Germany

Received 5 December 2008; received in revised form 16 August 2009; accepted 26 August 2009

Abstract

Ten years after the first observation of large-scale wave-like coronal disturbances with the EIT instrument aboard *SOHO*, the most crucial questions concerning these "EIT waves" are still being debated controversially – what is their actual physical nature, and how are they launched? Possible explanations include MHD waves or shocks, launched by flares or driven by coronal mass ejections (CMEs), as well as models where coronal waves are not actually waves at all, but generated by successive "activation" of magnetic fieldlines in the framework of a CME. Here, we discuss recent observations that might help to discriminate between the different models. We focus on strong coronal wave events that do show chromospheric Moreton wave signatures. It is stressed that multiwavelength observations with high time cadence are particularly important, ideally when limb events with CME observations in the low corona are available. Such observations allow for a detailed comparison of the kinematics of the wave, the CME and the associated type II radio burst. For Moreton-associated coronal waves, we find strong evidence for the wave/shock scenario. Furthermore, we argue that EIT waves are actually generated by more than one physical process, which might explain some of the issues which have made the interpretation of these phenomena so controversial.

Keywords: Sun; Solar corona; Solar flares; Coronal mass ejections; Waves; Shocks

1. Introduction

Signatures of large-scale wavelike disturbances propagating through the solar atmosphere have first been observed in the solar chromosphere in the 1960s (Moreton, 1960). These *Moreton waves* appear as arc-shaped fronts propagating away from flaring active regions (ARs) at speeds of the order of 1000 $\mathrm{km\,s^{-1}}$. The fronts are seen in emission in the center and in the blue wing of the Hα line, whereas in the red wing they appear in absorption, which is interpreted as a Doppler shift due to a depression of the chromosphere by an invisible agent (Moreton, 1964). In combination with their high speed, this was taken as evidence for the scenario that Moreton waves are just the ground-track of a dome-shaped MHD wavefront that expands through the corona and sweeps over the chromosphere (Uchida et al., 1973; and references therein). The same *MHD wave* can generate metric type II bursts when it steepens to a *shock* (Uchida, 1974), and it can excite filament oscillations (e.g. Eto et al., 2002). Originally the wave was considered as a flare-launched freely propagating blast wave, but in principle also a coronal mass ejection (CME) can launch such a wave, or alternatively create a driven disturbance.

A decade ago, the Extreme Ultraviolet Imaging Telescope (EIT; Delaboudinière et al., 1995) aboard *SOHO* first detected actual coronal signatures of large-scale propagating wave-like disturbances (Thompson et al., 1998). They were originally interpreted as the coronal counterpart of the chromospheric Moreton waves, and some events have been successfully modelled as fast-mode waves (Wang, 2000; Wu et al., 2001). However, it quickly turned out that EIT waves, as these disturbances came to be known, have rather different characteristics. They show a wider range of morphological patterns (cf. Klassen et al., 2000), ranging from sharp Moreton-like fronts to diffuse and irregular brightenings. They are significantly slower than Moreton

* Tel.: +49 331 7499 208; fax: +49 331 7499 352.
E-mail address: awarmuth@aip.de

0273-1177/$36.00 © 2009 COSPAR. Published by Elsevier Ltd. All rights reserved.
doi:10.1016/j.asr.2009.08.022

waves, with typical propagation speeds of only a few 100 $km\,s^{-1}$. Moreover, they show a large velocity spread – the slowest disturbances propagate with only a few tens of $km\,s^{-1}$ (cf. Wills-Davey et al., 2007), which is significantly slower than both the sound and the Alfvén speed in the corona. Some EIT fronts seem to stop at coronal hole boundaries (e.g. Delannée and Aulanier, 1999; Delannée et al., 2007), and there are reports of rotating wavefronts (Attrill et al., 2007).

These observations have led to the development of some alternative models. In the *magnetic reconfiguration scenarios*, EIT waves are not waves in the physical sense, but rather the consequence of the reconfiguration of magnetic field lines during a CME lift-off (Delannée, 2000; Delannée and Aulanier, 1999). Depending on the magnetic topology, this mechanism can generate propagating as well as stationary bright fronts, either due to the generation of currents (Delannée et al., 2007; and references therein) or driven magnetic reconnection (Attrill et al., 2007) at the boundary between the expanding magnetic structure and the ambient field. Finally, both models can be combined, since an expanding CME will also generate waves. Such a scenario has been developed by Chen et al. (2002). Here, an erupting flux rope drives a piston shock. The top of this CME-driven shock generates the type II radio burst, while its legs extend down to the solar surface where they can produce Moreton waves. Simultaneously, behind the legs of the shock a plasma density enhancement is propagating at a lower speed (it may be even stationary). This feature is due to successive stretching or opening of closed field lines covering the erupting flux rope, and based on its velocity it is interpreted as the EIT wave. The Chen model thus explains the velocity discrepancy between Moreton and EIT waves by invoking two physically distinct disturbances.

Thus, 10 years after the discovery of EIT waves, the physical nature of these disturbances is still discussed controversially. Determining which of the competing models best conforms to reality requires accumulating as much information as possible about the wave events. Luckily, wave signatures have also been discovered in soft X-rays (SXR; Narukage et al., 2002; Khan and Aurass, 2002) and in chromospheric Helium I (HeI) filtergrams (Gilbert et al., 2001; Vršnak et al., 2002), opening up new channels of information. In this paper, we therefore combine two approaches: on the one hand, we study in detail the kinematics and perturbation evolution of coronal waves with the help of multiwavelength data set including Hα, extreme ultraviolet (EUV), soft X-rays (SXR), Helium I (HeI) and radio observations. On the other hand, we include significantly more events than is typical for in-depth case-studies. This allows us to study correlations between different wave parameters and possible wave sources.

2. Events and data sources

In this paper, we focus on coronal waves that show Moreton wave signatures. These waves may be regarded as the "large-amplitude limit" of the phenomenon, since it requires a stronger perturbation to perturb the dense chromosphere (cf. Warmuth et al., 2004b). Early in these events, also the coronal signatures of the disturbances tend to be more intense and coherent than in an average coronal wave event. This allows to measure the kinematics and profile evolution with sufficient accuracy. In addition, Hα data usually provide much better temporal cadence than coronal observations, and can be easily corrected for projection effects. These are the main reasons for the restriction to this subclass of events.

An in-depth search of various Hα data archives has turned up 27 Moreton wave events in the range from 1997 to 2006. The multiwavelength approach is crucial, since the image cadence of EIT (typically 12 min) is too low for a detailed study of the waves' kinematics. Besides EIT data (for 21 events), additional coronal observations in the SXR regime were available from *Yohkoh*/SXT (Tsuneta et al., 1991; 6 events) and *GOES*-SXI (Hill et al., 2005; Pizzo et al., 2005; 12 events). Full-disk Hα data were provided by the solar observatories at Kanzelhöhe (Otruba and Pötzi, 2003), Big Bear (Denker et al., 1999), Mauna Loa (the PICS instrument; Fisher et al., 1981; see also Gilbert et al., 2008), Hida (the FMT telescope[1]; Kurokawa et al., 1995; and the SMART telescope[2]; UeNo et al., 2004), Meudon (see Manoharan and Kundu, 2003; and references therein), and by the O-SPAN (Neidig et al., 1998) instrument. The cadence of Hα images is typically between 30 s and 3 min, which is significantly better than the cadence of the coronal observations. Additional chromospheric observations in the HeI line at 10,830 Åwere available from the CHIP instrument (Elmore et al., 1998) at Mauna Loa for 11 events.

The relation of the coronal waves with associated type II bursts was studied using dynamic radiospectra from the following radiospectrographs: Potsdam-Tremsdorf (Mann et al., 1992), Culgoora (Prestage et al., 1994), and the RSTN network of the US Air Force (Guidice et al., 1981).[3] Coronagraphic data for low heights was available for one event from the Mk-3 K-coronameter at Mauna Loa Solar Observatory (Fisher et al., 1981). The timing of the associated hard X-ray (HXR) bursts was derived from *CGRO*/BATSE (Fishman et al., 1989), *Yohkoh*/HXT (Kosugi et al., 1991) and *RHESSI* (Lin et al., 2002) data.

Table 1 shows an overview of the large-amplitude coronal wave events and some associated phenomena. Shown are the event date, the NOAA number of the source active region, *NOAA no.*, the coordinates and GOES importance of the associated flare, *flare loc.* and *flare imp.*, the linear speed of the associated CME in $km\,s^{-1}$, v_{lin}, and whether

[1] http://www.kwasan.kyoto-u.ac.jp/general/facilities/fmt/index_en.html.

[2] http://www.hida.kyoto-u.ac.jp/smart/.

[3] http://www.ngdc.noaa.gov/stp/SOLAR/ftpsolarradio.html#spectralgraphs.

Table 1
Overview of the large-amplitude coronal wave events and associated phenomena. For details see main text.

Date	NOAA no.	Flare loc.	flare imp.	CME v_{lin}	Hα wave	EUV wave	SXR wave	HeI wave
1997 September 24	8088	S31E19	M5.9	202	×	×		
1997 November 03	8100	S20W13	C8.6	227	×	×	×	
1997 November 03	8100	S20W15	M1.4	338	×	×	×	
1997 November 04	8100	S14W33	X2.1	785	×	×		
1997 November 27	8113	N17E63	X2.6	441	×	×	×	
1998 May 02	8210	S15W15	X1.1	938	×	×		
1998 August 08	8299	N13E74	M3.0		×			
1998 August 18	8307	N33W87	X4.9		×		–	
1998 August 19	8307	N32E75	X3.9	1543	×			–
1998 August 24	8307	N35E09	X1.0		×			×
1999 October 14	8731	N11E32	X1.8	1250	×	×		
2000 March 02	8882	S20W58	M6.5	835	×	×		
2000 March 03	8882	S15W60	M3.8	841	×	×	×	
2000 November 25	9236	N20W23	X1.9	671	×	×	–	×
2003October 28	10,486	S16E08	X17.2	2459	×	–		
2003 October 29	10,486	S15W02	X10.0	2029	×	×	×	×
2003 November 03	10,488	N10W82	X2.7	827	×	×	×	
2003 November 03	10,488	N08W77	X3.9	1420	×	×	×	
2003 November 04	10,486	S19W83	X28.0	2657	×	×	×	×
2004 July 13	10,646	N14W45	M6.7	607	×	×	×	×
2004 December 30	10,715	N03E48	M4.2	1035	×	×	×	×
2005 January 17	10,720	N15W25	X3.8	2548	×	×	–	
2005 August 02	10,794	S12E47	M4.2	580	×	×	×	×
2005 August 03	10,794	S11E36	M3.4	488	×	×	×	
2005 September 07	10,808	S06E89	X17.0	1417	×		×	×
2006 December 06	10,930	S06E63	X6.5		×		×	×
2006 December 14	10,930	S06W46	X1.5	1042	×	×	×	×

wavefronts were observed in Hα, EUV, SXR, or HeI. "x" means that wavefronts were detected, "–" means that no wave features were seen, and a blank space indicates that no or insufficient data were available.

It is evident from Table 1 that wave signatures are generally present in all available spectral bands, with a few exceptions that can be traced to insufficient data quality or cadence and infavorable viewing geometries. This implies that the physical disturbance that creates coronal waves has to be compressive and cannot be solely due to a temperature change. Moreover, the disturbance has to extend over a significant height range, from the base of the corona up to heights of over 100 Mm. Thus, the perturbation has to expand as a 3D structure.

Metric type II bursts were detected in all wave events. Thus the large-amplitude wave events are highly associated with propagating coronal shock waves. Flares are present in all events, and CMEs were detected in all cases where coronagraphic observations were available.

3. Results

3.1. Kinematics

The distances of the leading edges of the wavefronts from the center of the associated flare were measured along 10 great circles (see Warmuth et al., 2004a) for all EIT, SXR, Hα, and HeI wave fronts. An example of the resulting kinematical curves is shown in Fig. 1 for the well-studied event of 2003 November 3 (e.g. Vršnak et al., 2006). Note that the error bars on the distances represent the standard deviation of the 10 points measured on each wavefront. This is usually significantly larger than the intrinsic measurement error in each point, therefore the error bars for velocity and acceleration which will be shown below do not primarily represent an uncertainty due to measurement errors, but rather a range for the parameters given by the anisotropic propagation of the waves.

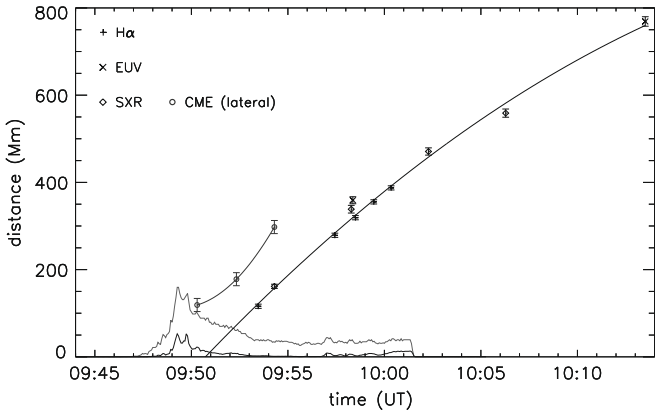

Fig. 1. Combined distance–time plot of the coronal wave 2003 November 3, including Hα, EIT, and SXI fronts. Also shown is the lateral expansion of the CME flank, as well as the HXR emission of the associated flare in the energy bands of 25–50 and 50–100 keV as measured by *RHESSI* (grey and black curves, respectively). The error bars represent the standard deviation of the 10 distance measurements for each front.

From this distance–time plot it is evident that EIT data alone are insufficient to study kinematics, since there are only two detected fronts. When we include the high-cadence Hα data, we note two things: both Moreton and EIT wavefronts are consistent with a single underlying disturbance, and this common perturbation is not propagating at a constant speed, but it is decelerating. However, the overlap between the observed distance ranges of Hα and EIT fronts is not very large, because Moreton waves can be traced only to a few 100 Mm from their origin. In this case, including the wavefronts observed by *GOES*-SXI solves the problem: they nicely tie together the distance ranges of Moreton and EIT waves since they can be observed both close and far from the source and have sufficient cadence. They conclusively show that indeed all signatures of the coronal wave are created by a single disturbance (see also Warmuth et al., 2005). Note that Moreton front actually seems to lag some 20–30 Mm behind the EIT and SXI fronts. This is due to projection effects (the coronal wave features are 3D structures extended in height and seen integrated along the line-of-sight, whereas the Moreton wave is a flat structure close to the solar surface) and the time the chromosphere needs to react to the coronal impulse. An MHD simulation by Chen et al. (2005) has derived a comparable offset between Moreton and SXR wavefronts.

We stress that *all* studied events show the same basic characteristics: the signatures in all wavelength ranges – Hα, HeI, EUV, and SXR – are consistent with a single underlying physical disturbance. In all cases, the disturbance is decelerating. This is seen from the combined kinematical curves as well as in the individual data sets from the various spectral channels. Moreover, there is a relation between the amount of deceleration and propagation speeds: faster waves tend to decelerate more strongly. This is shown in Fig. 2 for the average (i.e., linear) speed derived from the combined wavefronts from all spectral channels, $v_{lin,cb}$, and the average deceleration, a_{cb} (as given by 2^{nd} degree polynomial fits). Note that in one of the events, White and Thompson (2005) did not detect deceleration for a propagating wave imaged at 17 GHz with the Nobeyama radioheliograph. Contrasting to that, we found that the associated Moreton and EIT waves were in agreement with a common decelerating disturbance, but the wave was originally rather slow and showed thus only weak deceleration. The Nobeyama observations of the wave span only 4 min, and considering that these are synthesized images which do introduce some artifacts, it is easily conceivable that any weak deceleration has been missed.

These results confirm that the apparent "velocity discrepancy" of Moreton and EIT waves is merely an artifact: with its low cadence, EIT catches a wave only when it has already propagated to larger distances and has thus already decelerated, whereas in Hα, the wave is only visible close to the source, where it is still fast. Recent observations of a coronal wave with EUVI confirm this scenario (Long et al., 2008; Veronig et al., 2008). These facts do not support the model of Chen et al. (2002), where EIT and Moreton wave are two different phenomena. While it cannot be ruled out that slower disturbances trailing behind the faster waves are created by magnetic reconfiguration, the lack of observational detections implies that any such features would have to be significantly fainter than the ones associated with the main perturbation. This notion is supported by similar simulations by Pomoell et al. (2008) in which trailing disturbances are only found for very strong flux rope acceleration, and even in those cases they are not interpreted as the EIT wave.

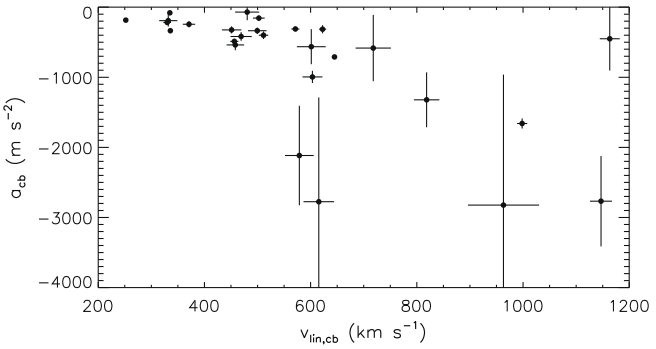

Fig. 2. Average deceleration versus mean propagation speed of the waves, derived from the combined kinematical curves using data from all available wavelength ranges. Note that all waves are decelerating.

Note that the apparent initiation of a filament oscillation that preceded the arrival of the EIT wave (Eto et al., 2002) has been quoted as evidence for the Chen scenario. Warmuth et al. (2004b) have interpreted this event in terms of a tilted coronal wavefront: since the filament is located higher up, the more tenuous upper – and thus less observable – parts of the wavefront will reach it first. Furthermore, determining at which time the filament actually begins to oscillate can be quite ambiguous, so that the possible errors can be much larger than the errors on the wavefronts. In any case, this single observation contrasts with the 27 events of the present study where all observable wavefronts are consistent with a single disturbance. Associated filament oscillations will be considered in a future publication.

The kinematics of the waves – deceleration and correlation of speed with the rate of deceleration – are characteristic for freely propagating shocks formed from large-amplitude fast-mode MHD waves, so-called simple waves (cf. Mann, 1995). The propagation speed of these disturbances is related to their amplitude. As they propagate, their amplitude decreases mainly due to geometric expansion, and consequently they decelerate. Finally, the waves may decay to ordinary (i.e., linear) fast-mode waves.

3.2. Perturbation evolution

Besides kinematics, the evolution of the perturbation profile is the most basic characteristic of coronal waves. We study the evolution of the perturbation by measuring the intensity as a function of distance from the source,

averaged over the angle that the wavefronts span, and normalized by a pre-event (i.e., undisturbed) profile. Such intensity profiles were obtained both from Hα (21 events) and EIT data (24 events). From the profiles, we obtain the FWHM thickness of the wavefronts and their maximum intensity (i.e., amplitude) by fitting the profiles with Gaussians.

The majority of events, both in Hα and EUV, shows a clear trend of broadening wavefronts with increasing distance (or time), and practically all waves show a decrease of amplitude with increasing distance. This confirms the results of a more limited study by Warmuth et al. (2004b). The trends are also evident when we combine the data from all events, as shown in Fig. 3. In Fig. 3(a), we see that the FWHM of the Moreton and EIT wavefronts blend into another in the distance range of 100–500 Mm, another indication that both signatures are created by a common disturbance. In Fig. 3(b), the decrease in amplitude is very evident for both EIT and Moreton waves, however, here the two populations do not blend into each other. This is due to the different generation mechanisms: the Hα signatures are primarily due to Doppler shifts in the chromosphere, while the brightness of the EIT fronts is due to an increase of density (and possibly also temperature) in the corona.

The fact that the EUV signatures are a more direct signature of the disturbance allows us to make inferences on its physical nature. Assuming that the emission enhancement is solely due to an increase in density, it follows that initially many waves have compression factors of larger than 1.2. In the case of a real wave generating this disturbance, it would have to be a large-amplitude, and hence nonlinear, wave. Alternatively, if significant heating is involved, this can also only be generated by a large-amplitude pulse in the wave model.

All characteristics of the perturbation profiles and their evolution – the large amplitudes, the broadening and weakening of the profile – are consistent with large-amplitude simple waves, or with freely propagating shocks formed by a steepening of these simple waves (see Vršnak and Lulić, 2000a; Žic et al., 2008). Moreover, the kinematics also fits this picture (see Section 3.1): initially, the simple wave (or shock) has a sharp profile with a large-amplitude, and hence it is fast. Due to geometric expansion, which increases the length along the wavefront, and the fact that the leading edge propagates faster than the trailing one, the profile broadens, the amplitude decreases, and consequently the speed drops.

It should be noted that Wills-Davey (2006) has found a rather constant pulse width for a coronal wave observed with *TRACE*. This has been interpreted as supporting the interpretation that EIT waves are solitons (Wills-Davey et al., 2007). However, this event was much weaker than the waves studied here.

3.3. Relation with type II bursts

We have already seen that the high-amplitude wave events are highly associated with coronal shocks that generate metric type II bursts. Using timing and kinematics, we can get a deeper understanding of their actual physical relation. Fig. 4(a) shows a histogram of the time difference between the start of the type II burst and the first observation of a wavefront. The distribution clearly shows that the onset of coronal wavefronts and type II-producing shock waves is synchronized – in 94% of cases, both phenomena appear within 5 min.

Comparing the kinematics of coronal waves and type II bursts is somewhat more ambiguous. Radiospectral observations only yield the speed of the burst source relative to the density gradient, and even this speed is dependent on the coronal density model used. Radioheliographic observations can be used to constrain the density model and to obtain the plane-of-sky speed of the source, too (see e.g. Vršnak et al., 2006). However, these observations are only available for a minority of the studied events. We therefore adopt the single Newkirk model (Newkirk, 1961) for all events. Based on actual coronal density measurements, Cho et al. (2007) have recently shown that this model is a good approximation to the real density distribution (Magdalenić et al., 2008). Fig. 4(b) shows the initial type II speed versus the first measured Moreton wave

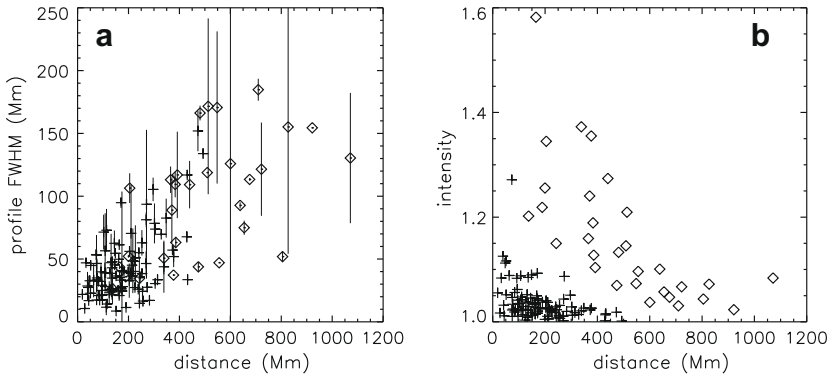

Fig. 3. (a) FWHM of the perturbation profile versus distance for Moreton (*crosses*) and EIT waves (*diamonds*). (b) Maximum intensity of the perturbation profile versus distance for Moreton and EIT waves.

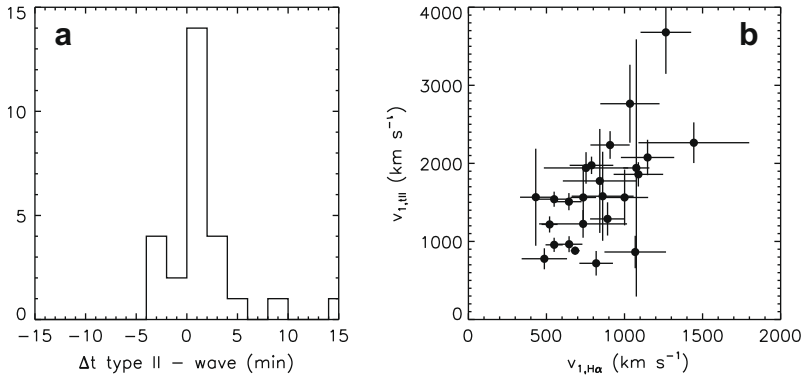

Fig. 4. (a) Histogram of the time lag Δt between the start of the type II burst and the first observation of a wavefront (in minutes). (b) Initial type II speed, $v_{1,II}$, versus first measured Moreton wave speed, $v_{1,H\alpha}$.

speed. There is a clear correlation – faster type II bursts are associated with faster waves. Initially, the type bursts are about twice as fast as the Moreton waves.

Considered together, association, timing, and kinematics suggest that both coronal waves and type II-producing coronal shocks are signatures of the same disturbance, or alternatively are generated by the same driver. This is consistent with the wave/shock model, where at least a certain part of the expanding coronal wave can steepen to a supercritical (i.e., radio-producing) shock. Radioheliographic observations have revealed that type II burst sources can be cospatial with the wavefronts (e.g. Khan and Aurass, 2002), which supports the former scenario. The magnetic reconfiguration scenario, on the other hand, is not expected to provide such a close correspondence in time, space and kinematics.

3.4. Relation with flares and CMEs

Studying the flares and CMEs associated with coronal waves is of particular importance since this can provide insights into the physical nature of the disturbances as well as into the possible generation mechanisms. Generally, three different phenomena have been proposed as possible wave sources:

- flares: they could launch a freely propagating blast wave by generating a pressure pulse (e.g. Vršnak and Lulić, 2000b; Vršnak and Cliver, 2008);
- small-scale ejecta (e.g. flare spray, erupting plasmoids, etc.): these phenomena could generate an initially driven disturbance which later continues to propagate freely (e.g. Klein et al., 1999);
- CMEs: they offer three different possibilities – they could generate: (1) a piston-driven or bow shock; (2) an only initially driven shock that continues to propagate freely after the acceleration phase (Gilbert and Holzer, 2004); (3) successive brightenings due to the opening, reconfiguration, or reconnection of magnetic field lines (e.g. Delannée et al., 2007).

Previous studies of potential generation mechanisms of coronal waves have focused on association with flares and CMEs (e.g. Biesecker et al., 2002; Cliver et al., 2005). These studies found that while most EIT waves are associated with flares, many of the associated flares have SXR intensities below C class. This raises the question of what makes these events special. After all, there are many more small flares than EIT waves. Moreover, there are stronger flares that are not associated with waves (Chen, 2006). Since EIT waves are rather highly associated with CMEs (Biesecker et al., 2002; Cliver et al., 2005), it has been proposed that actually the CMEs are the central ingredient to wave production. The same case has been made for type II bursts (e.g. Cliver et al., 1999).

As our analysis has not been completed yet, we here report only some first results on the relation between the large-amplitude wave events and associated flares and CMEs (small-scale ejecta will not be discussed here). With regard to flares, we have studied the relative timing of the HXR burst – which is the signature for nonthermal energy input – and the wave launch. Fig. 5(a) shows a histogram of the time difference between the first observation of a wavefront and the peak of the associated HXR burst. The distribution is centered on zero time lag, and 89% of the waves first occur within ± 4 min with respect to the HXR peak. This suggests that the wave launch might be connected to the impulsive energy release in the flare. However, it has been shown that the acceleration profile of CMEs tends to peak during this period, too (e.g. Kahler et al., 1988; Zhang et al., 2001; Maričić et al., 2007; Temmer et al., 2008). Therefore, we can not make a distinction between a flare-related and a CME-related scenario based on timing alone. Another possibility is energetics – a stronger flare should be associated with a stronger pressure pulse, leading to a faster disturbance. Fig. 5(b) shows the initial Moreton wave speed versus the peak *GOES* SXR intensity (i.e., flare importance). Larger flares tend to be really associated with faster waves, but the correlation is not very strong. Again, as bigger flares are associated with more energetic CMEs, we cannot really claim that the correlation with *GOES* flux hints at a flare-related wave launch.

Correlations in timing and energetics can of course also be studied for CMEs, but the most revealing source of

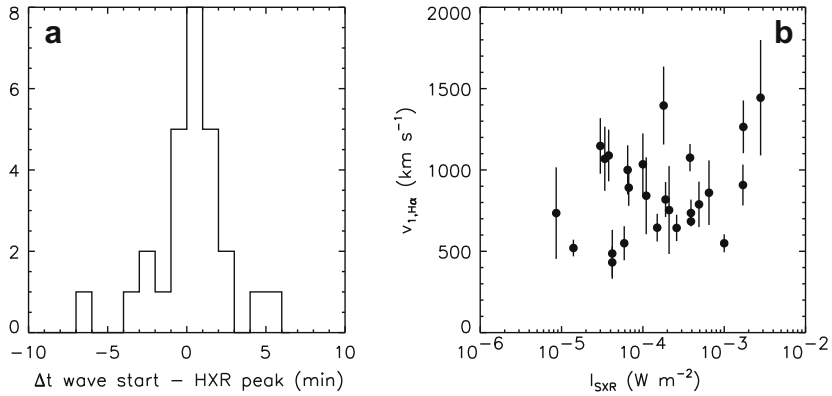

Fig. 5. (a) Histogram of the time lag Δt between the first observation of a wavefront and the peak of the associated HXR burst(in minutes). (b) First measured Moreton wave speed, $v_{1,H\alpha}$, versus peak *GOES* flare intensity, I_{SXR}.

information is their kinematics in relation to the kinematics of the coronal wave. In other words, the location of the CME front (or flank) with respect to the wave, and how it evolves in time, should enable us to determine whether the wave can actually be generated by the expanding CME. However, there are two complications for this kind of study. Firstly, we need coronagraphic observations of the CME in the low corona, which is where most of the acceleration is happening. In addition, the flanks of the CME, which propagate laterally, are actually more relevant to the generation of coronal waves than the radial expansion of the CME. Such observations are generally not available from space-based coronagraphs. Secondly, to minimize projection effects, the wave event should be located close to the solar limb, and the propagation direction should be along the solar limb. This allows an unambiguous comparison of wave and CME kinematics throughout the whole event.

These requirements result in a very limited number of events that are suitable for analysis. The first example was 2003 November 3, where the early expanding CME was imaged by *GOES*-SXI (see Vršnak et al., 2006). Analysis of this event has shown that the CME flank is actually propagating *ahead* of the coronal wave by some 100 Mm (see Fig. 1). Another example is shown in Fig. 6: for the Moreton wave of 1998 August 19, coronagraphic data from the Mk-3 coronagraph was available. In this event, the CME flank is initially also observed to propagate ahead of the wave. At some point the CME flank decelerates and becomes essentially stationary, while the wave continues its propagation and finally even overtakes the now stationary CME flank (note that the same behavior has been reported for some type II burst; see Wagner and MacQueen, 1983; Gary et al., 1984). This behavior rules out both the scenario of a shock driven by the expanding CME front as well as a magnetic reconfiguration model, at least in these two. However, a CME-related origin can not be excluded completely: it is still possible that the wave is a freely propagating disturbance that was only driven at the onset of the CME expansion, not necessarily by the CME front, but rather by substructures within the expanding CME. Further studies of more events will be necessary to determine the validity of this scenario.

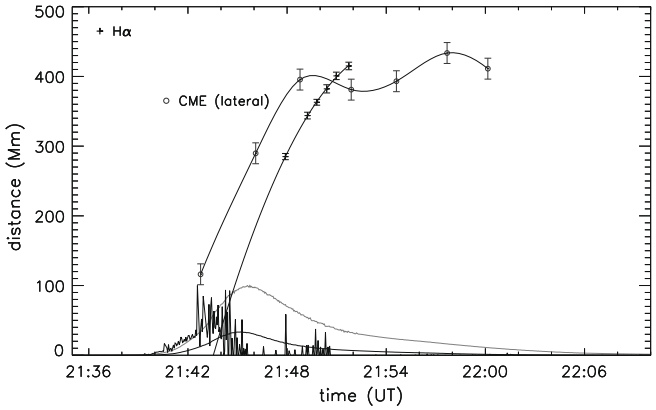

Fig. 6. Distance–time plot of the Moreton wave 1998 August 19. Also shown is the lateral expansion of the CME flank, as well as the *GOES* SXR emission of the associated flare and its derivative (spiky curve).

3.5. Evidence for physically different classes of events

From our study of large-amplitude coronal waves, we have found strong evidence for the wave/shock model. However, as summarized in Section 1, several observed characteristics of EIT waves cannot be reproduced by this model. This discrepancy could be resolved if the large-amplitude events we have studied are physically different from the "common" EIT waves. Indeed, it is intriguing to note that studies which focus on Moreton waves tend to find evidence for the wave/shock model, whereas those concentrating on EIT waves seem to be gravitating to alternative models. Thompson et al. (2000) have already pointed out that several physical mechanisms could play a role in Moreton/EIT wave events. The notion of different classes of EIT waves has been suggested by Biesecker et al. (2002) and Zhukov and Auchère (2004). Thus, is there any quantitative evidence for different classes of EIT waves?

Thompson and Myers (2009) have measured the propagation speeds of 176 EIT waves. Fig. 7(a) shows a histo-

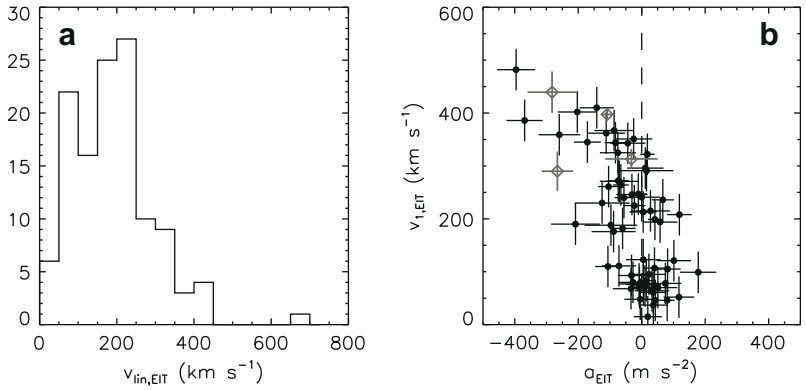

Fig. 7. (a) Histogram of the first measured EIT wave speeds, $v_{1,EIT}$, from Thompson and Myers (2009) wave catalogue. (b) First measured EIT wave speed, $v_{1,EIT}$, versus mean EIT wave acceleration, a_{EIT} (note that waves with $a_{EIT} < 0$ are decelerating). Dots represent values from Thompson and Myers (2009), while diamonds depict the wave events of this study.

gram of the average projected EIT wave speeds (obtained from linear fits). While the distribution peaks between 200 and 250 km s^{-1}, there is an extended tail up to a few 100 km s^{-1}, as well as a secondary maximum below 100 km s^{-1}. This indicates that there may be more than one distinct component in this distribution.

Let us study this possibility by looking at the kinematical characteristics of the waves in more detail. In Fig. 7(b), we have plotted the initial EIT wave speed, $v_{1,EIT}$, versus the average acceleration, a_{EIT} (obtained from 2nd degree polynomial fits; note that waves with $a_{EIT} < 0$ are decelerating). The error bars are derived from assuming a possible distance measurement error of 20 Mm. We note that all waves with initial speeds higher than 300 km s^{-1} are all decelerating, while slower waves show either acceleration or deceleration. Moreover, the amount of deceleration is larger for faster waves, while no such correlation is observed for the slower events. While the crosses in Fig. 7(b) denote the values from Thompson and Myers (2009), the diamonds denote the EIT waves of the present study. It is evident that our large-amplitude events are consistent with the high-speed population of Thompson and Myers (2009) sample. As judging from their kinematics, the high-amplitude, fast EIT waves seem to form a distinct population. The correlation between the amount of deceleration and initial speed are again consistent with large-amplitude simple waves or shocks.

In contrast, no systematic kinematical behavior is evident for the slower waves. It is well possible that these events are not waves in a physical sense, but signatures of magnetic reconfiguration, or possibly some totally different physical process. Mixing together these different phenomena under the single category "EIT waves" would certainly be not appropriate, and may explain some of the apparent problems concerning the interpretation of coronal waves.

4. Conclusion

Using a multiwavelength data set, we have reported first results of a detailed study of the kinematics and perturbation evolution of a large sample of coronal wave events which do show chromospheric Moreton wave features. Most importantly, we have found that in all events, all different spectral signatures of the waves are consistent with a single physical disturbance. This disturbance, whatever it is, is decelerating in all cases. This straightforwardly explains the apparent "velocity discrepancy" between Moreton and EIT waves, confirming earlier results by Warmuth et al. (2001) and Warmuth et al. (2004a). Deceleration also implies that the model of Chen et al. (2002) – in which Moreton and EIT waves are generated by two different processes – is not required to explain Moreton and EIT waves. Indeed, the kinematical curves rule out this model in the events we have studied. We do not rule out that a secondary slow perturbation can be generated due to magnetic reconfiguration behind the primary wave, but if there is one, its observational signatures have to be much weaker, and thus it cannot be interpreted as the EIT wave. No secondary waves were detected in the events studied here, and no secondary wave was seen by Long et al. (2008), Veronig et al. (2008), and Gopalswamy et al. (2009) in the STEREO/EUVI wave event that had excellent cadence and sensitivity. However, Chen's model is able to reproduce the coronal dimming which is usually associated with the waves.

The perturbation evolution is characterized by a broadening of the perturbation profile of the wavefront and a decrease of amplitude with increasing time and distance. Taken together with the ubiquitous deceleration, this is evidence for a large-amplitude MHD wave (a so-called simple wave), or for a freely propagating shock formed by the steepening of such a nonlinear wave. Note that the recent detection of the reflection of a coronal wave at a coronal hole boundary with STEREO/EUVI has provided very strong evidence for the wave interpretation (Gopalswamy et al., 2009). Due to geometric expansion and the fact that the leading edge of such a perturbation propagates faster than the trailing one, the profile broadens, the amplitude decreases, and consequently the speed drops. A strong association with metric type II bursts, as well as correlations in timing and kinematics, suggests that at least parts of the disturbance can be shocked.

With regard to possible generation mechanisms, it was found that the wave launch is associated with the phase of impulsive energy input. However, it is difficult to distinguish between a flare-caused pressure pulse scenario and a CME-driven origin, since the acceleration profile of CMEs usually also peaks during this period. In that respect, comparing the propagation of limb waves with the kinematical curves of CME flanks as given by low coronal observations yields the most definite information. For two events, we found that the CME flanks are actually preceding the coronal wavefront. In one of the events, the CME flank comes to a halt at some point, while the propagation of the wave continues until it even overtakes the flank. This conclusively rules out the magnetic reconfiguration scenario of coronal waves (e.g. Delannée et al., 2007), as well as the interpretation as MHD shocks driven by the CME front of flank. The observations are still consistent with a flare-generated pressure pulse or with a perturbation that is only initially driven – by a CME, structures within a CME, or small-scale ejecta – and then continues as a freely propagating wave/shock. Distinguishing between these possibilities will require detailed studies of additional events. It is of course also possible that all these processes actually *do* generate disturbances (cf. Gilbert and Holzer, 2004), and which of these disturbances are observable could vary from event to event.

In summary, we find strong evidence for the wave/shock model, the perturbations being large-amplitude – possibly shocked – MHD waves. However, this model cannot explain all observational characteristics that were reported for EIT waves (cf. Section 1). Using the large EIT wave sample of Thompson and Myers (2009), we have for the first time shown quantitative evidence for different classes of waves that could be generated by distinct physical processes. The large-amplitude events we have studied – associated with both Moreton waves and type II bursts – seem to form a distinct class that is consistent with true waves/shocks. Mixing together this class with other events that may well not be real waves at all may be responsible causing some of the issues which have made the interpretation of these phenomena so controversial.

Acknowledgments

This work was supported by DLR under Grant No. 50 QL 0001. Hα data were provided by the high-speed Hα imaging system at Kanzelhöhe Solar Observatory. Mauna Loa Solar Observatory data is courtesy the High Altitude Observatory/National Center for Atmospheric Research. Hα data were also provided by the Global High Resolution Hα Network, operated by the Big Bear Solar Observatory, New Jersey Institute of Technology. Hα data are taken with the Flare Monitoring Telescope (FMT) at the Hida Observatory of Kyoto University, and we thank K. Shibata and S. Ueno for their support. Data from the Meudon Heliograph were kindly provided by J.-M. Malherbe (Paris Observatory). The Optical Solar Patrol Network (OSPAN) project is a collaboration between the Air Force Research Laboratory Space Vehicles Directorate and the National Solar Observatory. This study is based on data obtained at OAFA (El Leoncito, San Juan, Argentina) in the framework of the German-Argentinean HASTA/MICA Project, a collaboration of MPE, IAFE, OAFA and MPAe. Radiospectra were used with permission of Culgoora Solar Observatory, IPS Radio and Space Services, Bureau of Meteorology, Australia. *SOHO* is a project of international cooperation between ESA and NASA. We thank the NOAA Space Environment center for free access to SXI data which were obtained from the National Geophysical Data Center. *Yohkoh* is a mission of the Japanese Institute for Space and Astronautical Science.

References

Attrill, G.D.R., Harra, L.K., van Driel-Gesztelyi, L., Demoulin, P. Coronal "wave": magnetic footprint of a coronal mass ejection? ApJ 656, L101–L104, 2007.

Biesecker, D.A., Myers, D.C., Thompson, B.J., et al. Solar phenomena associated with "EIT waves". ApJ 569, 1009–1015, 2002.

Chen, P.F., Wu, S.T., Shibata, K., Fang, C. Evidence of EIT and Moreton waves in numerical simulations. ApJ 572, L99–L102, 2002.

Chen, P.F., Ding, M.D., Fang, C. Synthesis of CME-associated Moreton and EIT wave features from MHD simulations. SSR 121, 201–211, 2005.

Chen, P.F. The relation between EIT waves and solar flares. ApJ 641, L153–L156, 2006.

Cho, K.-S., Lee, J., Moon, Y.-J. A study of CME and type II shock kinematics based on coronal density measurement. A&A 461, 1121–1125, 2007.

Cliver, E.W., Webb, D.F., Howard, R.A. On the origin of solar metric type II bursts. SoPh 187, 89–114, 1999.

Cliver, E.W., Laurenza, M., Storini, M., Thompson, B.J. On the origins of solar EIT waves. ApJ 631, 604–611, 2005.

Delaboudinière, J.-P., Artzner, G.E., Brunaud, J., et al. EIT: extreme-ultraviolet imaging telescope for the SOHO mission. SoPh 162, 291–312, 1995.

Delannée, C., Aulanier, G. CME associated with transequatorial loops and a bald patch flare. SoPh 190, 107–129, 1999.

Delannée, C. Another view of the EIT wave phenomenon. ApJ 545, 512–523, 2000.

Delannée, C., Hochedez, J.-F., Aulanier, G. Stationary parts of an EIT and Moreton wave: a topological model. A&A 465, 603–612, 2007.

Denker, C., Johannesson, A., Marquette, W., et al. Synoptic Hα full-disk observations of the sun from bigbear solar observatory – I. Instrumentation, image processing, data products, and first results. SoPh 184, 87–102, 1999.

Elmore, D.F., Card, G.L., Chambellan, C.W., et al. Chromospheric helium imaging photometer (an instrument for high time cadence 1083-nm wavelength solar observations). Appl. Opt. 37, 4270–4276, 1998.

Eto, S., Isobe, H., Narukage, N., et al. Relation between a Moreton wave and an EIT wave observed on 1997 November 4. PASJ 54, 481–491, 2002.

Fisher, R.R., Lee, R.H., MacQueen, R.M., Poland, A.I. New Mauna Loa coronograph system. Appl. Opt. 20, 1094–1101, 1981.

Fishman, G.J., Meegan, C.A., Wilson, R.B., et al. In: Johnson, W.N. (Ed.), Proc. GRO Science Workshop, vol. 2, 1989.

Gary, D.E., Dulk, G.A., House, L., et al. Type II bursts, shock waves, and coronal transients – the event of 1980 June 29, 0233 UT. A&A 134, 222–233, 1984.

Gilbert, H.R., Thompson, B.J., Holzer, T.E., Burkepile, J.T., A comparison of CME-associated atmospheric waves observed in coronal

(19.5 nm) and chromospheric (He I 1083 nm and H-alpha 656 nm) lines, American Geophysical Union, Fall Meeting 2001, Abstract #SH12B-0746, 2001.
Gilbert, H.R., Holzer, T.E. Chromospheric waves observed in the He I spectral line ($\lambda = 10,830$ Å): a closer look. ApJ 610, 572–587, 2004.
Gilbert, H.R., Daou, A.G., Young, D., et al. The filament-Moreton wave interaction of 2006 December 6. ApJ 685, 629–645, 2008.
Gopalswamy, N., Yashiro, S., Temmer, M., et al. EUV wave reflection from a coronal hole. ApJ 691, L123–L127, 2009.
Guidice, D.A., Cliver, E.W., Barron, W.R., Kahler, S. The air force RSTN system. Bull. Am. Astron. Soc. 13, 553, 1981.
Hill, S.M., Pizzo, V.J., Balch, C.C., et al. The NOAA goes-12 solar X-ray imager (SXI) 1. Instrument, operations, and data. SoPh 226, 255–281, 2005.
Kahler, S.W., Moore, R.L., Kane, S.R., Zirin, H. Filament eruptions and the impulsive phase of solar flares. ApJ 328, 824–829, 1988.
Khan, J.I., Aurass, H. X-ray observations of a large-scale solar coronal shock wave. A&A 383, 1018–1031, 2002.
Klassen, A., Aurass, H., Mann, G., Thompson, B.J. Catalogue of the 1997 SOHO-EIT coronal transient waves and associated type II radio burst spectra. A&A Suppl. 141, 357–369, 2000.
Klein, K.-L., Khan, J.I., Vilmer, N., et al. X-ray and radio evidence on the origin of a coronal shock wave. A&A 346, L53–L56, 1999.
Kosugi, T., Masuda, S., Makishima, K., et al. The hard X-ray telescope (HXT) for the Solar-A mission. SoPh 136, 17–36, 1991.
Kurokawa, H., Ishiura, K., Kimura, G., et al. Observations of solar Hα filament disappearances with a new solar flare monitoring-telescope at hida observatory. J. Geomag. Geoelectr. 47, 1043–1052, 1995.
Lin, R.P., Dennis, B.R., Hurford, G.J., et al. The reuven ramaty high-energy solar spectroscopic imager (RHESSI). SoPh 210, 3–32, 2002.
Long, D.M., Gallagher, P.T., McAteer, R.T.J., Bloomfield, D.S. The kinematics of a globally propagating disturbance in the solar corona. ApJ 680, L81–L84, 2008.
Magdalenić, Vršnak, B., Pohjolainen, S., et al. A flare-generated shock during a coronal mass ejection on 24 December 1996. SoPh 253, 305–317, 2008.
Mann, G., Aurass, H., Voigt, W., & Paschke, J., Preliminary observations of solar type II bursts with the new radiospectrograph in Tremsdorf (Germany). In: Proceedings of the First SOHO Workshop, pp. 129–132, 1992.
Mann, G. On simple magnetohydrodynamic waves. J. Plasma Phys. 53, 109–125, 1995.
Manoharan, P.K., Kundu, M.R. Coronal structure of a flaring region and associated coronal mass ejection. ApJ 592, 597–606, 2003.
Maričić, D., Vršnak, B., Stanger, A.L., et al. Acceleration phase of coronal mass ejections: II synchronization of the energy release in the associated flare. SoPh 241, 99–112, 2007.
Moreton, G.E. Hα Observations of flare-initiated disturbances with velocities 1000 km/s. AJ 65, 494–495, 1960.
Moreton, G.E. Hα shock wave and winking filaments with the flare of 20 September 1963. AJ 69, 145, 1964.
Narukage, N., Hudson, H.S., Morimoto, T., et al. Simultaneous observation of a Moreton wave on 1997 November 3 in Hα and soft X-rays. ApJ 572, L109–L112, 2002.
Neidig, D., Wiborg, P., Confer, M., et al. The USAF improved solar observing optical network (ISOON) and its impact on solar synoptic data bases. In: Balasubramaniam, K.S., Harvey, J., Rabin, D. (Eds.), Synoptic Solar Physics, ASP Conf. Ser., vol. 140, p. 519, 1998.
Newkirk, G. The solar corona in active regions and the thermal origin of the slowly varying component of solar radio radiation. ApJ 133, 983–1013, 1961.
Otruba, W., Pötzi, W. The new high-speed Ha imaging system at Kanzelhhe Solar Observatory. Hvar Obs. Bull. 27, 189–195, 2003.
Pizzo, V.J., Hill, S.M., Balch, C.C., et al. The NOAA Goes-12 solar X-ray imager (SXI) 2 performance. SoPh 226, 283–315, 2005.
Pomoell, J., Vainio, R., Kissmann, R. MHD modeling of coronal large-amplitude waves related to CME lift-off. SoPh 253, 249–261, 2008.
Prestage, N.P., Luckhurst, R.G., Paterson, B.R., et al. A new radiospectrograph at Culgoora. SoPh 150, 393–396, 1994.
Temmer, M., Veronig, A.M., Vršnak, B., et al. Acceleration in fast Halo CMEs and synchronized flare HXR bursts. ApJ 673, L95–L98, 2008.
Thompson, B.J., Plunkett, S.P., Gurman, J.B., et al. SOHO/EIT observations of an Earth-directed coronal mass ejection on May 12, 1997. GRL 25, 2465–2468, 1998.
Thompson, B.J., Reynolds, B., Aurass, H., et al. Observations of the 24 September 1997 coronal flare waves. SoPh 193, 161–180, 2000.
Thompson, B.J., Myers, D.C. A catalog of coronal "EIT wave transients. ApJS 183, 225–243, 2009.
Tsuneta, S., Acton, L., Bruner, M., et al. The soft X-ray telescope for the SOLAR-A mission. Sol. Phys. 136, 37–67, 1991.
Uchida, Y., Altschuler, M.D., Newkirk Jr., G. Flare-produced coronal MHD-fast-mode wavefronts and Moreton's wave phenomenon. SoPh 28, 495–516, 1973.
Uchida, Y. Behavior of the flare produced coronal MHD wavefront and the occurrence of type II radio bursts. SoPh 39, 431–449, 1974.
UeNo, S., Nagata, S., Kitai, R., et al. Proc. SPIE 5492, 958–969, 2004.
Veronig, A.M., Temmer, M., Vršnak, B. High-Cadence observations of a global coronal wave by STEREO EUVI. ApJ 681, L113–L116, 2008.
Vršnak, B., Lulić, S. Formation of coronal MHD shock waves – I. The basic mechanism. SoPh 196, 157–180, 2000a.
Vršnak, B., Lulić, S. Formation of coronal MHD shock waves – II. The pressure pulse mechanism. SoPh 196, 181–197, 2000b.
Vršnak, B., Warmuth, A., Brajša, R., Hanslmeier, A. Flare waves observed in Helium I 10 830 Å. A link between Hα Moreton and EIT waves. A&A 394, 299–310, 2002.
Vršnak, B., Warmuth, A., Temmer, M., et al. Multi-wavelength study of coronal waves associated with the CME-flare event of 3 November 2003. A&A 448, 739–752, 2006.
Vršnak, B., Cliver, E.W. Origin of coronal shock waves. Invited review. SoPh 253, 215–235, 2008.
Wagner, W.J., MacQueen, R.M. The excitation of type II radio bursts in the corona. A&A 120, 136–138, 1983.
Wang, Y.-M. EIT waves and fast-mode propagation in the solar corona. ApJ 543, L89–L93, 2000.
Warmuth, A., Vršnak, B., Aurass, H., Hanslmeier, A. Evolution of two EIT/Hα Moreton waves. ApJ 560, L105–L109, 2001.
Warmuth, A., Vršnak, B., Magdalenić, J., et al. A multiwavelength study of solar flare waves. I. Observations and basic properties. A&A 418, 1101–1115, 2004a.
Warmuth, A., Vršnak, B., Magdalenić, J., et al. A multiwavelength study of solar flare waves. II. Perturbation characteristics and physical interpretation. A&A 418, 1117–1129, 2004b.
Warmuth, A., Mann, G., Aurass, H. First soft X-ray observations of global coronal waves with the GOES solar X-ray imager. ApJ 626, L121–L124, 2005.
White, S.M., Thompson, B.J. High-cadence radio observations of an EIT wave. ApJ 620, L63L66, 2005.
Wills-Davey, M.J. Tracking large-scale propagating coronal wave fronts (EIT Waves) using automated methods. ApJ 645, 757–765, 2006.
Wills-Davey, M.J., DeForest, C.E., Stenflo, J.O. Are "EIT Waves" fast-mode MHD waves? ApJ 664, 556–562, 2007.
Wu, S.T., Zheng, H., Wang, S., et al. Three-dimensional numerical simulation of MHD waves observed by the Extreme Ultraviolet Imaging Telescope. JGR 106, 25089–25102, 2001.
Zhang, J., Dere, K.P., Howard, R.A., et al. On the temporal relationship between coronal mass ejections and flares. ApJ 559, 452–462, 2001.
Zhukov, A.N., Auchère, F. On the nature of EIT waves, EUV dimmings and their link to CMEs. A&A 427, 705–716, 2004.
Žic, T., Vršnak, Temmer, M., Jacobs, C. Cylindrical and spherical pistons as drivers of MHD shocks. SoPh 253, 237–247, 2008.